ACS Synthetic Biology

pubs.acs.org/synthbio
Research Article

Simultaneous Detection of Multiple Analytes at Ambient Temperature Using Eukaryotic Artificial Cells with Modular and Robust Synthetic Riboswitches

Hajime Takahashi, Yuri Ikemoto, and Atsushi Ogawa*

Cite This: ACS Synth. Biol. 2025, 14, 771−780
Read Online

ACCESS | Metrics & More | Article Recommendations | Supporting Information

ABSTRACT: Cell-free systems, which can express an easily detectable output (protein) with a DNA or mRNA template, are promising as foundations of biosensors devoid of cellular constraints. Moreover, by encasing them in membranes such as natural cells to create artificial cells, these systems can avoid the adverse effects of environmental inhibitory molecules. However, the bacterial systems generally used for this purpose do not function well at ambient temperatures. We here encapsulated a eukaryotic cell-free system consisting of wheat germ extract (WGE) and a DNA template encoding an analyte-responsive regulatory RNA (called a riboswitch) into giant unilamellar vesicles (GUVs) to create eukaryotic artificial cell-based sensors that function well at ambient temperature. First, we improved our previously reported eukaryotic synthetic riboswitches and WGE for use in GUVs by chimerizing two internal ribosome entry sites and optimizing magnesium concentrations, respectively, both of which increased the expression efficiency in GUVs several fold. Then, a DNA template encoding one of these riboswitches followed by a reporter protein was encapsulated with the optimized GUV-friendly WGE. Importantly, our previously established versatile method allowed for the rational design of highly efficient eukaryotic riboswitches that are responsive to a user-defined analyte. In fact, we utilized this method to successfully create three types of artificial cells, each of which responded to a specific, membrane-permeable analyte with wide-range, analyte-dose dependency and high sensitivity at ambient temperature. Finally, due to their orthogonality and robustness, we were able to mix a cocktail of these artificial cells to achieve simultaneous detection of the three analytes without significant barriers.

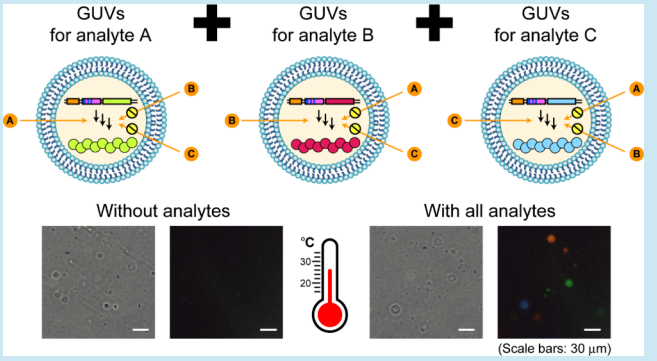

KEYWORDS: *artificial cell, biosensor, cell-free system, riboswitch, synthetic biology, wheat germ extract*

INTRODUCTION

Cell-free systems have recently attracted attention as fundamental elements for building up biosensors.[1−3] They contain components required for the translation of exogenously added mRNA templates (or in some cases for coupled transcription/translation of DNA templates), thereby allowing researchers to create cell-free system-based sensors (hereafter called cell-free sensors) merely by designing templates that promote the expression of easily detectable reporter proteins in response to analytes. In addition, cell-free sensors have many advantages over cell-based sensors, including their lack of bioethical or biohazard issues, easier preparation and handling, shorter response time, higher specificity and stability, ability to detect toxic analytes, and utility for the flexible design of gene circuits.[4] Although the absence of cell membranes might be expected to constitute a disadvantage since it could allow various environmental molecules (especially ions, nucleases, and proteases) to inhibit gene expression, liposomes can be used to encapsulate cell-free sensors and sequester them from the extracellular environment while still permitting the inflow of membrane-permeable molecules.[5,6] Such encapsulated cell-free sensors (i.e., artificial cell-based sensors) are expected to circumvent cumbersome and time-consuming sample-purification processes (and their associated losses) and allow for the direct detection of membrane-permeable analytes in unpurified samples.

In order for a cell-free sensor to recognize an analyte (as an input) and subsequently express a reporter protein (as an output), input-to-output signal transduction must be introduced. A promising candidate for this end is a molecule-responsive gene-regulatory RNA called a riboswitch.[7] The riboswitch is located in an untranslated region (UTR) of

Received: October 8, 2024
Revised: November 21, 2024
Accepted: November 26, 2024
Published: December 27, 2024

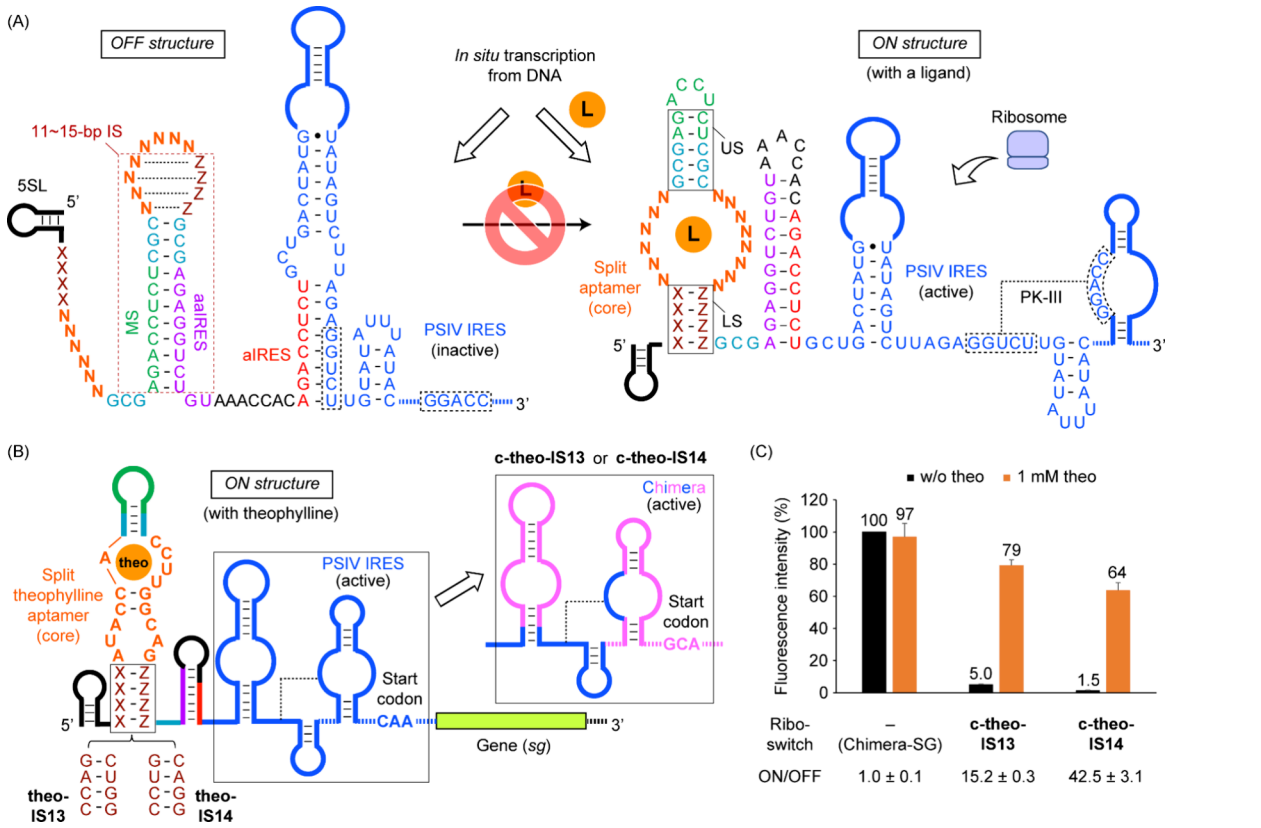

Figure 1. Construction of theophylline-responsive, eukaryotic kinetic ON-riboswitches with a highly efficient chimeric IRES between the PSIV and CrPV[GCA] IRESes. (A) Predicted switching mechanism of PSIV IRES-based kinetic ON-riboswitches designed by our versatile method. While the PSIV IRES is distorted by the aIRES to be inactive if the IS length is sufficiently long (left, OFF structure), it is kinetically trapped into the active structure with PK-III if formation of the aptamer/ligand complex occurs during transcription (before the aaIRES hybridizes to the MS) and induces that of the aaIRES/aIRES duplex (right, ON structure). The IS length in the OFF structure varies depending on the 3′-side LS sequence (ZZZZ), which hybridizes to the 5′-side LS (XXXX) in the ON structure. The 5′ terminal stem-loop structure (5SL) is added to enhance T7 transcription, stabilize transcripts, and prevent the eukaryotic canonical translation. (B) Replacement of the PSIV IRES with the chimeric IRES in two PSIV IRES-based riboswitches responsive to theophylline (**theo-IS13** and **theo-IS14**) to construct **c-theo-IS13** and **c-theo-IS14**, respectively. Only the predicted ON structure is shown due to space limitation. (C) Relative green fluorescence intensities of SG expressed from DNA templates encoding **c-theo-IS13** or **c-theo-IS14** before the SG gene at 26 °C for 3 h in the absence or presence of 1 mM theophylline (theo) in the GUV-free WGE-cIVTT system. The error bars represent the standard deviation (n = 4).

mRNA and consists of two domains: an aptamer and an expression platform. When the aptamer binds to its specific ligand molecule, conformational changes or alternative folding of the expression platform is induced, which turns expression of the downstream (or upstream) gene on or off. Although naturally occurring riboswitches respond only to endogenous metabolites in cells, it is possible to artificially construct a riboswitch responsive to a user-defined ligand by successfully inserting an *in vitro*-selected aptamer for the ligand into mRNA.[8] In fact, some natural or synthetic riboswitches have been used to create artificial cell-based sensors for detecting their ligand molecules (i.e., analytes).[9−14]

To date, however, all such sensors have been based on bacterial cell-free systems and riboswitches. Therefore, they have the drawback that detection has to be conducted at a relatively high temperature (around 37 °C), which is not suitable for on-the-spot sensing. We here focus on wheat germ extract (WGE),[15] a eukaryotic cell-free system, and eukaryotic riboswitches that function well in WGE. Importantly, the optimal temperature for expression in WGE is around 26 °C, which is within ambient and room temperature. Although the productivities of eukaryotic cell-free systems including WGE used to be much lower than those of bacterial ones, especially in batch mode, we recently developed a coupled *in vitro* transcription/translation (cIVTT) system for efficient batch reactions in WGE, the productivity of which was comparable to those of some bacterial cIVTT systems.[16] In addition, we have established several rational methods for engineering eukaryotic riboswitches with *in vitro*-selected aptamers.[17−28] One of them allows us to rationally construct and modulate riboswitches that upregulate internal ribosome entry site (IRES)-mediated translation through a kinetic trapping mechanism with high switching efficiency in the WGE-based cIVTT system.[27] In fact, several kinetic riboswitches (i.e., kinetically functioning riboswitches) designed with this method, each responding specifically to a different ligand, exhibited high induction ratios of >25 at moderate ligand concentrations. We have here further improved these modular kinetic riboswitches and the WGE-based cIVTT system toward higher expression efficiency in liposomes and then encapsulated the improved pairs to create eukaryotic artificial cell-based sensors, each expressing a specific reporter protein in response to the corresponding analyte, for simultaneous detection of multiple analytes at ambient temperature.

https://doi.org/10.1021/acssynbio.4c00696
ACS Synth. Biol. 2025, 14, 771−780

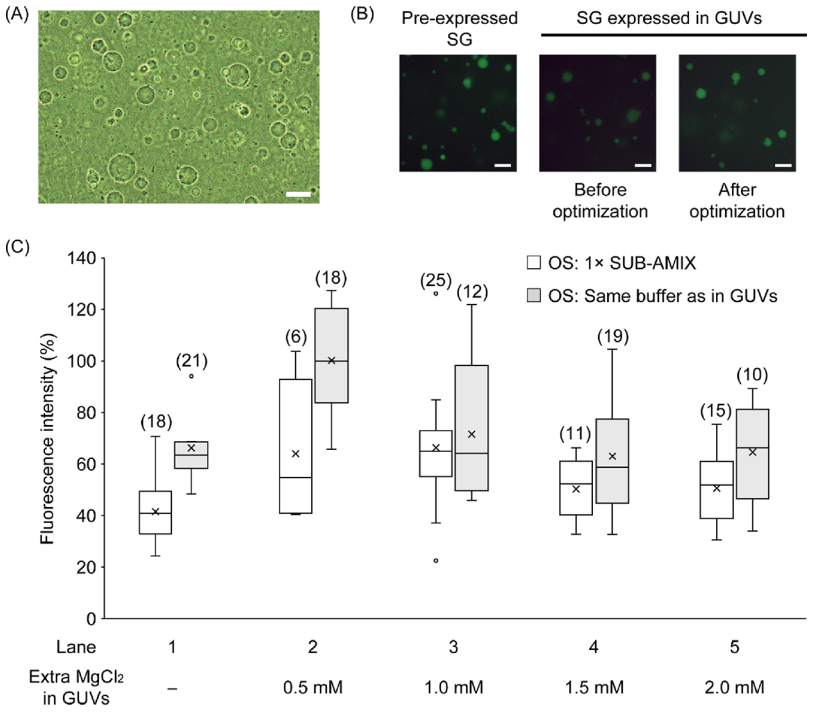

Figure 2. Optimization of WGE-based cIVTT in GUVs. (A) Phase-contrast image of GUVs prepared by an emulsion transfer method improved for encapsulating the WGE-based cIVTT system. (B) Representative green fluorescence images of the SG-positive control GUVs (left), which encapsulated SG that was pre-expressed from Chimera-SG at 26 °C for 3 h in the cIVTT system, and GUVs encapsulating Chimera-SG and the cIVTT system (with extra 0.5 mM $MgCl_2$ for the right image only) after incubation at 26 °C for 3 h under the preoptimized (center) or optimized (right) conditions. (C) Green fluorescence intensities of GUVs encapsulating Chimera-SG and the cIVTT system with various concentrations of extra $MgCl_2$ after incubation at 26 °C for 3 h in an OS consisting of the 1× SUB-AMIX buffer without (white bars) or with (gray bars) the same concentrations of $MgCl_2$ and NTPs as in the GUVs, relative to that of the SG-positive control GUVs. The numbers of the measured GUVs are shown in parentheses. Scale bars are 30 μm.

RESULTS AND DISCUSSION

Chimerization of PSIV and CrPV IRESes for Facile Design of Eukaryotic Kinetic Riboswitches with High Expression Efficiency. As described above, we recently developed a versatile method to rationally construct kinetic riboswitches that upregulate IRES-mediated translation efficiently in eukaryotic expression systems (Figure 1A).[27] This type of kinetic, upregulating riboswitch (i.e., ON-riboswitch) folds into an inactive OFF structure during transcription without its ligand (Figure 1A, left), while it folds into an active ON structure with the ligand (specifically, the ligand kinetically traps the riboswitch in its ON conformation), allowing the ribosome binding to the IRES and the subsequent translation of the downstream gene (Figure 1A, right). Importantly, the riboswitch can be easily optimized or fine-tuned simply by adjusting the length of the inhibitory stem (IS) in the proposed OFF structure (Figure 1A, left). Because these kinetic riboswitches require no post-transcriptional thermodynamic conformational change by their ligands, they are highly likely to show higher switching efficiency with low-to-moderate ligand concentrations than thermodynamic riboswitches, which function through an equilibrium mechanism. However, the IRES used in our previously constructed kinetic riboswitches was a less active one from the *Plautia stali* intestine virus (PSIV),[29] whereas we had already modified an IRES from cricket paralysis virus (CrPV) to create CrPV[GCA] IRES, an improved IRES showing several-fold higher translation efficiency in WGE.[30] Given the fact that higher translation efficiency in the ON state should be better for easy detection of the expressed protein, especially in artificial cells, the latter IRES seemed to be suitable for the construction of kinetic riboswitches in this study.

As to our initial reason for using the PSIV IRES to design the previous eukaryotic kinetic riboswitches, we had already identified two short sequences for regulating its activity—i.e., the anti-IRES (aIRES) and anti-aIRES (aaIRES) sequences—which deactivate (aIRES) and reactivate (aaIRES) the PSIV IRES by hybridization to the IRES and the aIRES, respectively (Figure 1A).[18] Although both the PSIV IRES and the CrPV IRES are in the same class of intergenic IRESes of *Cripaviruses*,[31] the sequence of the 5′-side pseudoknot III (PK-III), which should be targeted by the aIRES, is different between the two IRESes (Figure S1A,B). This means that we have to fully optimize another aIRES/aaIRES pair to construct kinetic riboswitches based on the more active CrPV[GCA] IRES. In addition, a modulator sequence (MS) for preventing the aaIRES from hybridizing to the aIRES in the OFF structure (Figure 1A, left) must be changed: Both ends of the changed MS would no longer be used as a part of an upper stem (US) of an aptamer core in the ON structure, unlike those of the original MS (5′ AG/CU 3′; Figure 1A, right), which could necessitate changes to the design method. We thus first prepared a chimera of the two IRESes by replacing the sequences of PK-III and its vicinity of the CrPV[GCA] IRES with those of the PSIV IRES (Figure S1C). As expected, Chimera-SG, a DNA template encoding this chimera IRES followed by the StayGold (a bright green fluorescent protein, hereafter called SG) gene,[32] exhibited expression efficiency

https://doi.org/10.1021/acssynbio.4c00696
ACS Synth. Biol. 2025, 14, 771−780

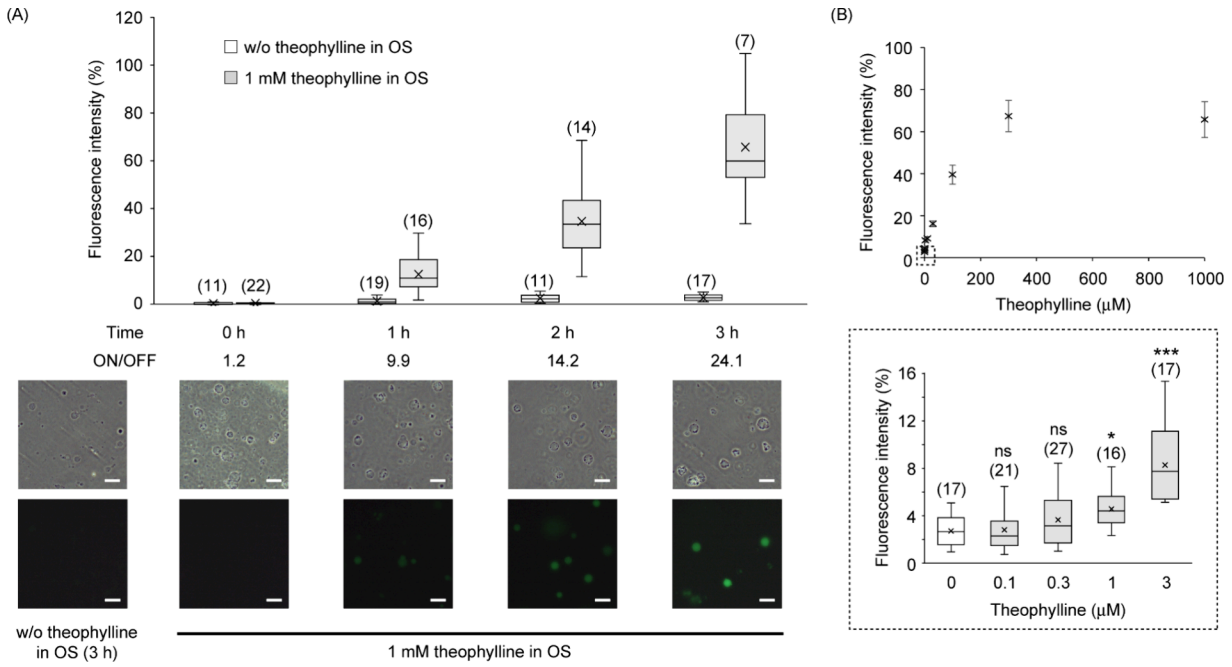

Figure 3. Theophylline-responsive artificial cells. (A) Green fluorescence intensities of GUVs encapsulating **c-theo-IS13**-encoding DNA (with the SG gene) and the GUV-friendly cIVTT system after incubation at 26 °C for 0, 1, 2, or 3 h under the optimized conditions in the absence or presence of 1 mM theophylline in the OS, relative to that of the SG-positive control GUVs. Representative phase-contrast and green fluorescence images of the GUVs and their average ON/OFF ratios are shown below the graph. Those of GUVs after a 3 h incubation without theophylline are also shown at far left for reference. (B) Green fluorescence intensities of the GUVs incubated at 26 °C for 3 h with various concentrations of theophylline. The error bars represent the standard error of the mean. Inset: The low-concentration region is shown in the box-and-whisker diagrams. $^{*}P < 0.05$, $^{***}P < 0.001$, ns (not significant, $P \geq 0.05$) compared to theophylline-free GUVs (two-tailed Dunnett's test). The numbers of the measured GUVs are shown in parentheses. Scale bars are 30 μm.

comparable to or slightly higher than CrPV-SG, another template encoding the original CrPV[GCA] IRES with the same gene, after a 3 h incubation at 26 °C in the WGE-based cIVTT system (Figure S1D,E). Incidentally, a similar tendency was also observed in liposomes (Figure S1F).

To confirm that this chimera successfully functions in our eukaryotic kinetic riboswitches, we next substituted it for the PSIV IRES in a kinetic riboswitch named **theo-IS14**,[27] which we previously optimized to efficiently respond to theophylline (a medication for asthma) in the WGE-based cIVTT system by applying our versatile method to an *in vitro*-selected, theophylline-binding aptamer (Figure 1B).[33] Additionally, the same substitution was conducted in a variant with a 1-bp shorter IS, **theo-IS13**,[27] which showed greater leakage without theophylline but higher expression with 1 mM theophylline (up to slightly lower than that of a riboswitch-free positive control). When DNA templates encoding either one of these chimeric riboswitches (**c-theo-IS14** and **c-theo-IS13**) before the SG gene were incubated at 26 °C for 3 h in the absence or presence of 1 mM theophylline in the WGE-based cIVTT system, they showed ON/OFF induction ratios of 42.5 ± 3.1 and 15.2 ± 0.3, respectively (Figure 1C), which were comparable to those of the original PSIV IRES-based riboswitches with the same gene (Figure S2) or other genes.[27] It should be noted that, despite their comparable high responsiveness to the ligand, the expression efficiencies were several fold higher than those by the original riboswitches. In addition, these results indicate that the chimeric IRES could be used instead of the PSIV IRES in thermodynamic riboswitches to enhance their expression efficiencies.[18,19,22,24−26]

Encapsulating the WGE-Based cIVTT System into Natural Cell-Sized Liposomes without Impairing Its Activity. We previously confirmed that the WGE-cIVTT system also functioned well within a millimeter-sized supergiant liposome (a supergiant unilamellar vesicle: SGUV) without a loss of productivity.[16,34,35] However, the larger the size of the liposome, the smaller the surface area per volume becomes and the lower amounts of an external analyte per volume pass through the surface (i.e., the phospholipid bilayer membranes), which would lead to lower responsiveness of riboswitches within the liposome. Nonetheless, when the liposome becomes too small, it is difficult to observe the protein expression within it. Therefore, we decided to use a natural cell-sized liposome (a giant unilamellar vesicle: GUV) as a container for the WGE-based cIVTT system.[5] WGE-encapsulating GUVs were prepared by using a manual water-in-oil (W/O) emulsion transfer with reference to a previously described method of preparing GUVs containing a bacterial cIVTT system.[36] Because the original method gave considerably aggregated liposomes with lipid lumps, we improved some conditions such as the phospholipid concentration in oil solution, the volume ratio of W/O emulsions to the oil solution, and the transfer speed to successfully prepare dispersed WGE-encapsulating GUVs with diameters of 10−30 μm (Figure 2A). We then used this improved method to encapsulate the WGE-based cIVTT system with the positive control DNA, Chimera-SG. When the resulting GUVs were incubated at 26 °C for 3 h using an expression buffer (1× SUB-AMIX) as an outer solution (OS), they exhibited detectable green fluorescence though their brightness was, on average, approximately 40% of the brightness of SG-positive control

https://doi.org/10.1021/acssynbio.4c00696
ACS Synth. Biol. 2025, 14, 771−780

GUVs, which encapsulated SG that was pre-expressed outside the GUVs under the same conditions (Figure 2B, left vs center; Figure 2C, lane 1, white bar). We speculated that this reduction of expression efficiency was due to considerable trapping of the magnesium ions required for the cIVTT reactions by phosphate groups of the phospholipids composing the inner membrane of GUVs.[37] As expected, additions of extra $MgCl_2$ (0.5−2.0 mM) to the cIVTT solution improved the expression efficiency 1.3−1.8-fold in GUVs (Figure 2C, white bars). In addition, when we changed the OS to 1× SUB-AMIX with the same concentrations of $MgCl_2$ and NTPs as those in the inner solution,[38] the expression efficiency was further improved (Figure 2C, gray bars): The efficiency at 0.5 mM extra $MgCl_2$ was the best and was comparable to that of the SG-positive control GUVs (Figure 2B, left vs right; Figure 2C, lane 2, gray bar).

Artificial Cells with a Eukaryotic Riboswitch Function That Respond to Theophylline. Having successfully optimized the conditions for encapsulating the WGE-based cIVTT system into GUVs without impairing its activity, we next encapsulated this GUV-friendly eukaryotic cell-free system (i.e., one including 0.5 mM extra $MgCl_2$) with either of the DNA templates encoding the theophylline-responsive chimeric riboswitches constructed above (**c-theo-IS13** or **c-theo-IS14**; Figure 1B). When we observed the GUVs after 3 h of incubation at 26 °C in the absence of theophylline in the optimized OS, faint green fluorescence was detected in GUVs encapsulating **c-theo-IS13**-encoding DNA (2.7% on average compared to the SG-positive control GUVs; Figure 3A and Figure S3A), while there was almost no fluorescence in those with **c-theo-IS14**-encoding DNA (0.78%; Figure S3A), similar to the results in bulk reactions outside GUVs (Figure 1C). However, unlike in the bulk reactions, the fluorescence in the GUVs encapsulating **c-theo-IS14**-encoding DNA was unfortunately comparable to the limit of detection (LOD) for SG (0.74%), which was calculated from the average fluorescence intensity plus three times the standard deviation of similarly incubated GUVs encapsulating only the GUV-friendly cIVTT system (blank $+3\sigma$). In fact, more than half of the measured GUVs encapsulating **c-theo-IS14**-encoding DNA showed fluorescence lower than this limit (Figure S3A). This means that higher concentrations of theophylline would be required for the expression of detectable amounts of SG within GUVs than in bulk reactions. In contrast, all fluorescence from GUVs with **c-theo-IS13**-encoding DNA was just barely above the limit. Therefore, we decided to use the latter GUVs to investigate their responses to theophylline. As a result of incubation at 26 °C in the presence of 1 mM theophylline, these GUVs gradually fluoresced over time, exhibiting fluorescence as strong as 66%, on average, of that in the SG-positive control GUVs in 3 h (Figure 3A). It should be noted that this relatively high expression ratio was only slightly lower than in bulk reactions under the same ON condition (79% at 1 mM theophylline relative to the positive control, Chimera-SG; Figure 1C). Given the fact that this riboswitch functions in a kinetic trapping mechanism (i.e., its ligand is required during transcription to regulate gene expression), these results indicate that theophylline permeated through GUV membranes reasonably rapidly. In contrast, the expression ratio under the OFF condition was lower in GUVs than outside them, which led to a 1.6-fold higher average ON/OFF induction ratio of 24.1 at 1 mM theophylline.

We then investigated the sensitivity of GUVs encapsulating **c-theo-IS13**-encoding DNA against theophylline. As shown in Figure 3B, the average fluorescence intensity increased in a manner dependent on the concentrations of theophylline from 1 to 300 μM. This sensitivity or dose dependency was identical to that of **theo-IS14** with 1-bp longer IS in bulk reactions.[27] In contrast, the minimum concentration of theophylline at which GUVs with **c-theo-IS14**-encoding DNA responded was as high as 100 μM (Figure S4). This result confirms that our selection criteria for the riboswitch used in the GUVs were correct: Expression within GUVs must be detectable (i.e., higher than the LOD) even under the OFF condition. Incidentally, when we encapsulated **c-theo-IS13**-encoding DNA with the same concentrations of theophylline as those outside the GUVs, the dose dependency was similar to that observed when theophylline was added only to the outside (Figure S5). These results clearly support our expectation that theophylline can diffuse into the inside of GUVs at a relatively high rate.

To also confirm that the vesicle membranes can sequester an encapsulated cell-free biosensor from inhibitory molecules, we added Ca^{2+} or RNase A to unencapsulated **c-theo-IS13**-encoding DNA in bulk reactions or to the theophylline-responsive GUVs (i.e., artificial cells) encapsulating the same DNA. As expected, these inhibitory molecules considerably inhibited the expression of the former naked DNA as well as that of the positive control, Chimera-SG (Figure S6A). In contrast, they did not significantly affect the performance of the latter artificial cells, reflecting the high barrier effect of the membranes (Figure S6B). These results suggest that this type of artificial cell could be used to detect a membrane-permeable analyte in biological or environmental samples.[13]

Artificial Cells with Eukaryotic Riboswitch Functions That Respond to Other Analytes. To validate our strategy for constructing artificial cells with a eukaryotic riboswitch function, we next sought to build up artificial cells that respond to tetracycline (an antibiotic) or ASP2905 (a promising drug for neurological diseases), both of which are membrane-permeable.[39,40]

In terms of the former analyte, we previously constructed an efficient, PSIV-IRES-based kinetic riboswitch responsive to tetracycline, **tc-IS12**, by using our design method with an *in vitro*-selected aptamer that binds to tetracycline,[41] as in the case of **theo-IS14**.[27] However, considering the results of the theophylline-responsive riboswitches, a variant with a 1-bp shorter IS, **tc-IS11**,[27] was also chosen as a candidate. We thus first replaced the PSIV IRES in these two riboswitches with the chimeric IRES (**c-tc-IS12** and **c-tc-IS11**; Figure S7A). Incidentally, these chimeric riboswitches were fused to the mScarlet-I3 (a bright red fluorescent protein, hereafter called mScI3) gene so that we could evaluate the expression efficiency independent from SG in experiments of simultaneous detection later (*vide infra*).[42] When we incubated DNA templates encoding one of them at 26 °C for 3 h in the absence or presence of 100 μM tetracycline in the GUV-free WGE-based cIVTT system, **c-tc-IS12** and **c-tc-IS11** showed ON/OFF induction ratios of 84.6 ± 7.5 and 31.6 ± 3.7, respectively (Figure S7B), which were comparable to those of the original riboswitches with another reporter gene.[27]

We then encapsulated one of the DNA templates with the GUV-friendly cIVTT system into GUVs. As expected, GUVs encapsulating **c-tc-IS12**-encoding DNA showed almost no red fluorescence even after a 3 h incubation at 26 °C in the absence of tetracycline: The average fluorescence was 0.27% of

https://doi.org/10.1021/acssynbio.4c00696
ACS Synth. Biol. 2025, 14, 771−780

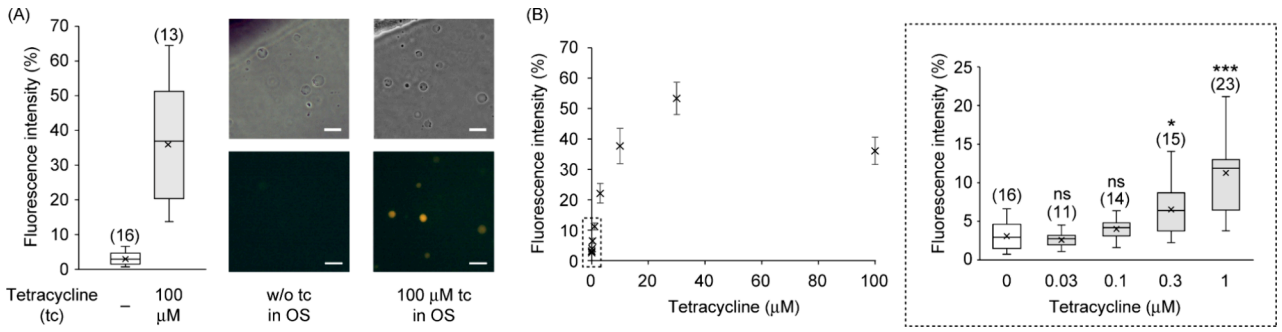

Figure 4. Tetracycline-responsive artificial cells. (A) Red fluorescence intensities of GUVs encapsulating **c-tc-IS11**-encoding DNA (with the mScI3 gene) and the GUV-friendly cIVTT system after a 3 h incubation at 26 °C under the optimized conditions in the absence or presence of 100 μM tetracycline (tc) in the OS, relative to that of the mScI3-positive control GUVs. Representative phase-contrast and red fluorescence images of the GUVs are shown on the right. (B) Red fluorescence intensities of the GUVs incubated at 26 °C for 3 h with various concentrations of tetracycline. The error bars represent the standard error of the mean. Inset: The low-concentration region is shown in the box-and-whisker diagram. *P < 0.05, ***P < 0.001, ns (not significant, $P \geq 0.05$) compared to tetracycline-free GUVs (two-tailed Dunnett's test). The numbers of the measured GUVs are shown in parentheses. Scale bars are 30 μm.

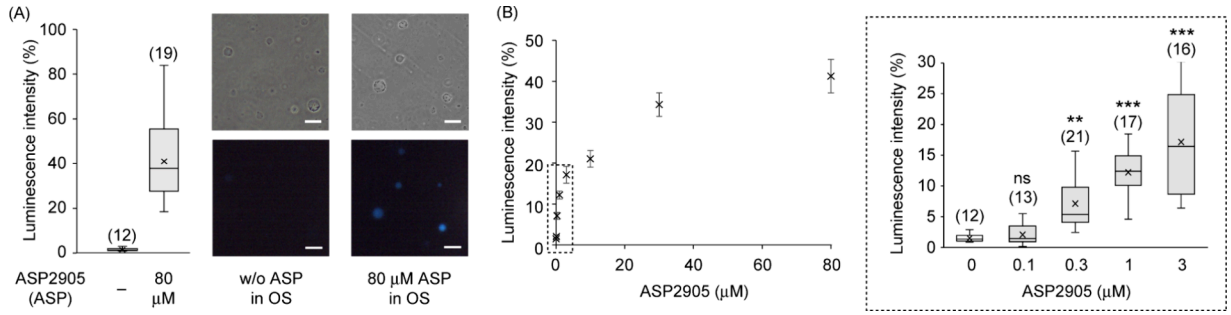

Figure 5. ASP2905-responsive artificial cells. (A) Luminescence intensities of GUVs encapsulating **c-ASP-IS12**-encoding DNA (with the nLuc gene) and the GUV-friendly cIVTT system after a 3 h incubation at 26 °C under the optimized conditions in the absence or presence of 80 μM ASP2905 (ASP) with 2% DMSO in the OS, relative to that of the nLuc-positive control GUVs. Representative phase-contrast and blue luminescence images of the GUVs are shown on the right. (B) Luminescence intensities of the GUVs incubated at 26 °C for 3 h with various concentrations of ASP2905 (all with 2% DMSO). The error bars represent the standard error of the mean. Inset: The low-concentration region is shown in the box-and-whisker diagram. **P < 0.01, ***P < 0.001, ns (not significant, $P \geq 0.05$) compared to ASP2905-free GUVs (two-tailed Dunnett's test). The numbers of the measured GUVs are shown in parentheses. Scale bars are 30 μm.

that for mScI3-positive control GUVs (encapsulating mScI3 expressed from Chimera-mScI3, which is a gene substitution variant of Chimera-SG; Figure S3B). This fluorescence intensity was much lower than the LOD for mScI3 (blank +3σ = 0.60%), and indeed, most of the measured GUVs did not reach this limit. In contrast, GUVs encapsulating **c-tc-IS11**-encoding DNA emitted detectable fluorescences (3.1% on average), all of which were above the limit (Figure 4A and Figure S3B). We thus incubated the latter GUVs at 26 °C for 3 h in the presence of 100 μM tetracycline to investigate their responses. The results showed that they exhibited moderate fluorescence, corresponding to 36%, on average, of that in the mScI3-positive control GUVs (Figure 4A). Although this expression ratio was not much lower than that in bulk reactions under the same ON condition (53% at 100 μM tetracycline relative to Chimera-mScI3; Figure S7B), the expression ratio under the OFF condition was slightly higher, unlike in the case of the theophylline-responsive GUVs, so that the average ON/OFF induction ratio decreased 3-fold by the encapsulation, down to 11.7 at a tetracycline concentration of 100 μM. Nonetheless, a slightly lower concentration of tetracycline (30 μM) induced more expression in GUVs: The expression ratio increased up to 53% with an ON/OFF induction ratio of 17.3 (Figure 4B). Given the fact that ∼300 μM tetracycline is required to inhibit WGE-based cIVTT of Chimera-mScI3 in bulk reactions (300 μM tetracycline decreased the expression efficiency to 57%, while 100 μM had no effect), these results indicate that tetracycline was somewhat (∼3-fold) concentrated in GUVs. In addition, by virtue of the much stronger affinity of the tetracycline aptamer implanted into the riboswitch,[41] the sensitivity of these GUVs against tetracycline was higher than that of the theophylline-responsive GUVs (Figure 4B): They responded to as low as 0.3 μM tetracycline with an ON/OFF ratio of 2.1, which is comparable to the responsiveness of **tc-IS12** with 1-bp longer IS in bulk reactions.[27]

To construct riboswitches responsive to the second analyte (ASP2905), we used the chimeric IRES from the beginning. Specifically, according to our design method,[27] an *in vitro*-selected aptamer binding to ASP2905 was inserted in split form instead of the theophylline- or tetracycline-binding aptamer,[43] and its lower stem (LS) sequences were varied so that the IS length was 12, 13, or 14 bp (**c-ASP-IS12**, **c-ASP-IS13**, or **c-ASP-IS14**, respectively; Figure S8A). Note that the nanoluciferase (nLuc) gene was here chosen to be regulated by these three riboswitches,[44] for the same reason that the mScI3 gene was chosen for the tetracycline-responsive riboswitches. When we incubated DNA templates encoding one of the riboswitches at 26 °C for 3 h in the absence or presence of 80 μM ASP2905 (with 2% DMSO in both cases) in the GUV-free

https://doi.org/10.1021/acssynbio.4c00696
ACS Synth. Biol. 2025, 14, 771−780

WGE-based cIVTT system (and then treated them with furimazine, a substrate of nLuc), two of the three riboswitches (**c-ASP-IS12** and **c-ASP-IS13**) were found to respond to ASP2905, with ON/OFF induction ratios of 13.8 ± 3.6 and 18.9 ± 1.1, respectively (Figure S8B). In contrast, the other one, **c-ASP-IS14**, showed no response, probably because the sequence of a part of the 3′-side LS and its vicinity (5′ UCAGC 3′) hybridized to the 5′ end of the IRES (5′ GCUGA 3′) to trap the IRES into a somewhat distorted structure under both the ON and OFF conditions (Figure S8A, parentheses).

The two kinds of ASP2905-responsive riboswitch-encoding DNAs were then separately encapsulated with the GUV-friendly cIVTT system into GUVs. The resulting GUVs were first incubated at 26 °C for 3 h in the absence of ASP2905 (but with 2% DMSO for a fair comparison) and then supplemented with furimazine. As for GUVs encapsulating **c-ASP-IS13**-encoding DNA, their average luminescence intensity was 0.68% of that in nLcu-positive control GUVs (encapsulating nLuc expressed from Chimera-nLuc, another gene substitution variant of Chimera-SG), which was comparable to the LOD for nLuc (blank +3σ = 0.70%), but the luminescence of individual GUVs was mostly below this limit (Figure S3C). In contrast, the luminescence from GUVs encapsulating **c-ASP-IS12**-encoding DNA was slightly brighter on average (1.5%), with all the individual values being above the limit (Figure 5A and Figure S3C), meaning that these GUVs were more suitable for biosensors. When they were incubated at 26 °C for 3 h in the presence of 80 μM ASP2905 (with 2% DMSO) and then treated with furimazine, they emitted bright blue luminescence corresponding to 41% of that in the nLuc-positive control GUVs (Figure 5A). This expression ratio was slightly lower than that in bulk reactions under the same ON condition (53% at 80 μM ASP2905 relative to Chimera-nLuc; Figure S8B), indicating that the membrane permeability of ASP2905 (and furimazine) is moderately high. In addition, the lower expression ratio under the OFF condition made the ON/OFF induction ratio about 2-fold higher, 27.3 on average at 80 μM ASP2905, compared with that in bulk reactions. Since ASP2905 has both high membrane permeability and high affinity to its aptamer,[43] the sensitivity of these GUVs against ASP2905 was comparable to that of the tetracycline-responsive GUVs: The luminescence increased in a dose-dependent manner from 0.3 to 80 μM (Figure 5B).

Simultaneous Detection of Multiple Analytes Using a Cocktail of Artificial Cells Responsive to Them. We finally utilized the three types of GUVs (i.e., artificial cells) encapsulating riboswitch-encoding DNA, each of which responds to different analytes (theophylline, tetracycline, or ASP2905) and expresses the corresponding protein (SG, mScI3, or nLuc, respectively), to detect the analytes simultaneously at ambient temperature. After confirming their orthogonality to nonanalytes (Figure S9), a cocktail of the GUVs was incubated at 26 °C for 3 h in the absence or presence of 300 μM theophylline, 30 μM tetracycline, and 30 μM ASP2905, the concentrations at which the corresponding GUVs showed the highest or comparable responses. As shown in Figure 6, whereas only faint fluorescence or luminescence was observed without any analytes, three types of relatively strong light (green fluorescence from SG, red fluorescence from mScI3, and blue luminescence from nLuc) were emitted from the corresponding GUVs in the presence of all the analytes, though their intensities were on the whole lower than those in single analyte detection with one type of GUV. The

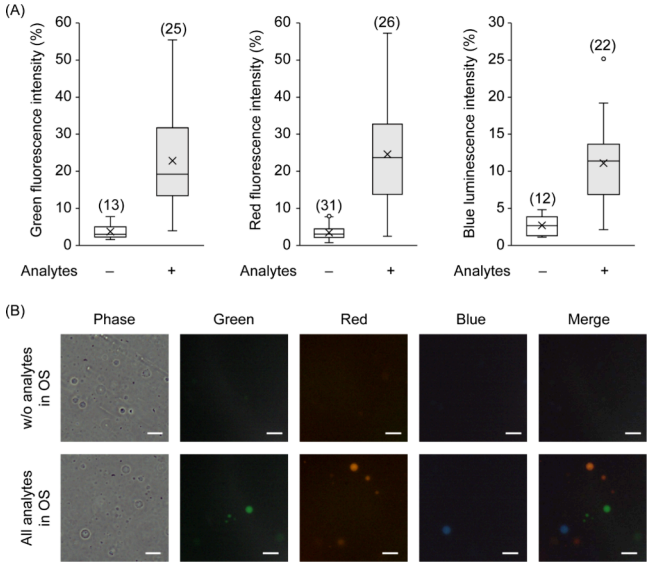

Figure 6. Simultaneous detection of multiple analytes using a cocktail of the three artificial cells responsive to them. (A) Green fluorescence (left), red fluorescence (center), and blue luminescence (right) intensities of the corresponding GUVs after a 3 h incubation at 26 °C under the optimized conditions in the absence or presence of 300 μM theophylline (theo), 30 μM tetracycline (tc), and 30 μM ASP2905 (ASP) in the OS, relative to those of the corresponding positive control GUVs. The reason that a low concentration of ASP2905 (with a low composition of DMSO: 0.75%) was used was that more than 1% DMSO slightly activated the theophylline-responsive GUVs even without theophylline (Figure S9A). The analyte-free OS also contained 0.75% DMSO. The numbers of the measured GUVs are shown in parentheses. (B) Representative phase-contrast, fluorescence (green and red), luminescence (blue), and merged images of the GUVs in panel A. Scale bars are 30 μm.

reason for the lower intensities was probably that the total amount of the analytes was large enough to inhibit cIVTT reactions. In fact, the intensities recovered as the total amount decreased (Figure S10), and the experiments also confirmed that any two of the three analytes induced emission of only the corresponding two types of GUVs in the cocktail. In addition, the theophylline dose dependency of the corresponding GUVs in the cocktail was comparable to that of the theophylline-responsive GUVs alone, even in the presence of the other two analytes (Figure S11). These results clearly reflect the high robustness of the artificial cells, which is derived from the riboswitches within them.

CONCLUSIONS

We here successfully created artificial cell-based sensors that can detect external analytes without the adverse effects of environmental inhibitory molecules and emit light with an intensity depending on their concentrations at ambient temperature. These are natural cell-sized GUVs encapsulating mainly two components: a WGE-based cIVTT system optimized for GUVs and a DNA template encoding a reporter protein under the control of a eukaryotic synthetic riboswitch (with the chimerized, efficient IRES) that functions there by a kinetic trapping mechanism with high expression and switching efficiencies. The eukaryotic cell-free system and riboswitch allow the artificial cells to operate well at ambient temperature, in contrast to the generally used bacterial ones.[9−14] In addition, our unique and versatile method enables us to rationally

https://doi.org/10.1021/acssynbio.4c00696
ACS Synth. Biol. 2025, 14, 771−780

construct efficient kinetic riboswitches with *in vitro*-selected aptamers for user-defined analytes.[27] We utilized these advantages to demonstrate simultaneous detection of three small molecules (theophylline, tetracycline, and ASP2905) at ambient temperature with a cocktail of three types of artificial cells, each of which contains a synthetic kinetic riboswitch that responds to one of the three analytes and expresses its specific reporter protein (SG, mScI3, and nLuc, respectively). It should be noted that these artificial cells showed high orthogonality and robustness, which are derived from the synthetic riboswitches. By obtaining aptamers specifically binding to other membrane-permeable analytes (and their specific reporter genes), we could realize a greater variety of orthogonal riboswitches and artificial cells with the riboswitches. In addition, coexpression of pore-forming proteins or transporters within GUVs would allow us to target hydrophilic, membrane-impermeable small analytes,[10−12,45] though engineering of the membrane proteins might be required to prevent undesired small molecules from entering the GUVs.

METHODS

Synthetic Nucleic Acids. Primers for PCR were purchased from Eurofins Genomics (Tokyo) or Thermo Fisher Scientific (Tokyo). All of the plasmids used were also artificially synthesized and sequenced by outsourcing. The sequences of primers and two pMK-based synthetic plasmids (Thermo Fisher Scientific), pCrPV[GCA]-His-SG and pCPc1-mScI3, are described in the Supporting Information. Those of the other four synthetic plasmids, pCrPV-IRES, pTheo5-PSIV-IRES, pEU-nLuc-Venus, and pHis-SRY-YPet, have been reported elsewhere.[21,24,30,46]

Preparation of DNA Templates. For preparation of the PSIV IRES-encoding templates, a 5′ segment encoding the PSIV IRES and a 3′ segment encoding the SG gene with a 3′ UTR were first sequentially PCR-amplified with PrimeSTAR MAX DNA polymerase (Takara Bio, Ohtsu, Japan) from pTheo5-PSIV-IRES and pCrPV[GCA]-His-SG, respectively. The two segments digested by *Spe* I were then ligated with Ligation high Ver. 2 (Toyobo, Osaka, Japan) to construct the first core DNA, PSIV-SG (Table S1).[27,47] For the nLuc-encoding templates, a 5′ segment encoding the CrPV[GCA] IRES and a 3′ segment encoding the nLuc gene were similarly PCR-amplified from pCrPV-IRES and pEU-nLuc-Venus, respectively. A ligation product between them (pre-CrPV-nL) obtained as described above was amplified and further fused to another 3′ segment (amplified from pHis-SRY-YPet) encoding almost the same 3′ UTR as those used for the other genes by using *Xho* I and the ligation kit to prepare another core DNA, CrPV-nL (Table S1). DNA templates for the WGE-based cIVTT system were constructed by using pCrPV[GCA]-His-SG, pCPc1-mScI3, or one of the two core DNAs above as the first template in sequential PCRs (Table S2). All PCR products in the sequential PCRs, except those in the final PCR, were agarose-gel-purified with a NucleoSpin Gel and PCR Clean-up kit (Takara Bio) and then used as templates in the next PCR. The final PCR products were simply purified with the same kit and quantified by absorbance at 260 nm. The sequences of DNA templates used for preparation of the three types of artificial cells with efficient eukaryotic riboswitch functions are described in the Supporting Information. Incidentally, although the length of 3′ UTRs that the resulting DNA templates encode is as short as ∼250 nt, we confirmed that their expression efficiencies were comparable to or slightly higher than those of DNA templates with longer 3′ UTRs in the cIVTT system, unlike in conventional translation from mRNA templates in WGE.[46]

Preparation of the WGE-Based cIVTT Reaction Solution. A total of 10 μL of mixture was prepared, basically consisting of 5 nM DNA template, 2.5 U/μL T7 RNA polymerase (Takara Bio), an additional 1.5 mM NTPs/$MgCl_2$ mix (0.375 mM each of NTPs and 1.5 mM $MgCl_2$), 40 ng/μL creatine kinase (CK), 1× SUB-AMIX (containing 2.7 mM $Mg(OAc)_2$, 1.2 mM ATP, and 0.25 mM GTP), and 20 v/v% WEPRO1240 (WGE).[16] The last three components (CK, SUB-AMIX, and WEPRO1240) were part of the WEPRO1240 Expression Kit (CellFree Sciences, Ehime, Japan). In some experiments, ligand molecules, extra $MgCl_2$, $CaCl_2$, and/or RNase A was included in the reaction solutions. For GUV-free cIVTT reactions (i.e., bulk reactions), the mixture was directly incubated at 26 °C for 3 h.

Encapsulation of the Reaction Solution into GUVs. 1-Palmitoyl-2-oleoyl-*sn*-glycero-3-phosphocholine, POPC (FUJIFILM Wako, Osaka, Japan), was dissolved in ethanol (as a safer alternative to more widely used chloroform) to a concentration of 100 mg/mL. A 12 μL portion of this POPC solution was mixed with 200 μL of nuclease- and protease-free mineral oil (Sigma-Aldrich, Tokyo) and incubated at 80 °C for 1 h to evaporate the ethanol. The resulting ethanol-free solution was centrifuged at 18,000*g* for 10 min at r.t., and only the supernatant was recovered to exclude undissolved POPC. Then, 10 μL of a WGE-based cIVTT reaction solution prepared as described above was added to 150 μL of the recovered POPC-containing oil solution in a 1.7 mL tube. This tube was rubbed against a tube rack about five times to generate W/O emulsions and incubated at 4 °C for 10 min.[48] The whole solution including the emulsions was layered onto 200 μL of an OS composed of 1× SUB-AMIX without or with an additional 1.5 mM NTPs/$MgCl_2$ mix and extra $MgCl_2$, the concentration of which was the same as in the reaction solution. The layered solution was then centrifuged at 13,500*g* for 30 min at 4 °C to generate GUVs. To establish positive controls, each protein (SG, mScI3, or nLuc) expressed from DNA encoding the riboswitch-free chimeric IRES and the corresponding gene (Chimera-SG, Chimera-mScI3, or Chimera-nLuc, respectively) in a 10 μL bulk reaction was similarly encapsulated in GUVs using only 1× SUB-AMIX as the OS. Incidentally, serially diluted reaction solutions with a cIVTT solution devoid of DNA templates were used to create calibration curves. The resulting GUVs were recovered by piercing the tube bottom (where the GUV pellet appeared) with an 18-gauge needle. For preparation of the GUV cocktail, each type of the recovered GUVs (from 5 tubes) was further concentrated 3-fold with centrifugation (13,500*g* for 3 min at 4 °C), and all the types were mixed in equal volumes.

Observation and Evaluation of GUVs. A total of 10 μL of the recovered GUVs (or the cocktail) was mixed with an equal volume of newly prepared OS without or with various concentrations of ligand molecules (in the presence of $CaCl_2$ or RNase A in some experiments) and then incubated at 26 °C for 3 h. For the positive controls, the recovered GUVs were just washed once with 1× SUB-AMIX to remove unencapsulated proteins. When evaluating the nLuc activity, 3 μL of the incubated (or washed) GUV solution was mixed with an equal volume of 1× SUB-AMIX with 4% DMSO and 2% Nano-Glo Luciferase Assay Substrate containing furimazine (Promega,

https://doi.org/10.1021/acssynbio.4c00696
ACS Synth. Biol. 2025, 14, 771−780

Tokyo), and half of the mixture was placed on a depression slide. For simultaneous detection, the same slide was also used for the subsequent fluorescence evaluations. When evaluating only the fluorescence intensities, 3 μL of the incubated (or washed) GUV solution was directly analyzed. The phase-contrast, fluorescence, and luminescence images were acquired using a fluorescence microscope (CKX53-22FL/PH; Olympus, Tokyo) equipped with a CMOS camera (CS-67C; Bitran, Gyoda, Japan). The camera temperature was set to −10 °C. For observation of green fluorescence (from SG) and red fluorescence (from mScI3), U-FYFP and standard U-FGW-like mirror units (Olympus) were used, respectively. Incidentally, green fluorescence of tetracycline is considerably reduced by the use of the former mirror unit: The green fluorescence of 30 μM tetracycline was below the LOD for SG. The exposure time (with a 16-fold gain) was 3, 1, or 5 s for SG, mScI3 or nLuc, respectively. The sizes and brightness of GUVs were analyzed using monochrome images with ImageJ software (NIH). The relative fluorescence and luminescence intensities were calculated by referring to size-dependent calibration curves drawn with the corresponding positive control GUVs containing serially diluted reaction solutions. Note that only GUVs with diameters of 10.7−17.6 μm were selected for the calculation because the R^2 value of each calibration curve was greater than 0.99 in this range. When using the GUV cocktail, each GUV was assigned to one of the three types based on its light emission and used only to calculate the corresponding light intensity.

Evaluation of GUV-Free cIVTT Reactions. The expression efficiencies of cIVTT in bulk reactions outside GUVs were evaluated directly by measuring either the fluorescence intensities of expressed fluorescent proteins or the luminescence intensity of expressed nLuc with a plate reader (ARVO X2; PerkinElmer, Yokohama, Japan), as previously described.[16,21] The excitation/emission wavelengths used were 485/535 and 544/590 nm for SG and mScI3, respectively.

■ ASSOCIATED CONTENT

Supporting Information

The Supporting Information is available free of charge at https://pubs.acs.org/doi/10.1021/acssynbio.4c00696.

Sequences of primers and plasmids used in PCRs; sequences of DNA templates for preparation of artificial cells with efficient eukaryotic riboswitch functions; Figure S1: chimerization of the PSIV IRES and the CrPV[GCA] IRES; Figure S2: PSIV IRES-based riboswitches responsive to theophylline; Figure S3: determination of whether the protein expression can be detected in GUVs encapsulating riboswitch-encoding DNA after a 3 h incubation in the absence of analytes; Figure S4: green fluorescence intensities of GUVs encapsulating **c-theo-IS14**-encoding DNA after a 3 h incubation in the presence of low concentrations of theophylline; Figure S5: green fluorescence intensities of GUVs encapsulating **c-theo-IS13**-encoding DNA and various concentrations of theophylline after a 3 h incubation with the same concentrations of theophylline as inside the GUVs; Figure S6: tolerance of the theophylline-responsive GUVs to inhibitory molecules; Figure S7: chimeric IRES-based riboswitches responsive to tetracycline; Figure S8: chimeric IRES-based riboswitches responsive to ASP2905; Figure S9: confirmation of orthogonality of the three types of artificial cells; Figure S10: simultaneous detection of two of the three analytes using the GUV cocktail; Figure S11: green fluorescence intensities of the theophylline-responsive GUVs in the cocktail after a 3 h incubation in the presence of various concentrations of theophylline, 30 μM tetracycline, and 30 μM ASP2905; Table S1: primers and templates used for preparation of core DNA sequences; Table S2: primers and templates used for preparation of DNA templates for expression (PDF)

■ AUTHOR INFORMATION

Corresponding Author

Atsushi Ogawa − *Proteo-Science Center, Ehime University, Matsuyama, Ehime 790-8577, Japan;* orcid.org/0000-0001-5240-3395; Email: ogawa.atsushi.mf@ehime-u.ac.jp

Authors

Hajime Takahashi − *Proteo-Science Center, Ehime University, Matsuyama, Ehime 790-8577, Japan*

Yuri Ikemoto − *Proteo-Science Center, Ehime University, Matsuyama, Ehime 790-8577, Japan*

Complete contact information is available at: https://pubs.acs.org/10.1021/acssynbio.4c00696

Author Contributions

A.O. conceived the project. H.T. and A.O. designed the experiments and wrote the manuscript. All authors cooperatively performed the experiments and discussed the results.

Notes

The authors declare no competing financial interest.

■ ACKNOWLEDGMENTS

This work was supported mainly by JSPS KAKENHI (24H01147 and 24K08603 to A.O.).

■ REFERENCES

(1) Silverman, A. D.; Karim, A. S.; Jewett, M. C. Cell-free gene expression: an expanded repertoire of applications. *Nat. Rev. Genet.* **2020**, *21*, 151−170.

(2) Wang, T.; Lu, Y. Advances, challenges and future trends of cell-free transcription-translation biosensors. *Biosensors* **2022**, *12*, 318.

(3) Garenne, D.; Haines, M. C.; Romantseva, E. F.; Freemont, P.; Strychalski, E. A.; Noireaux, V. Cell-free gene expression. *Nat. Rev. Methods Primers* **2021**, *1*, 49.

(4) Zhang, L.; Guo, W.; Lu, Y. Advances in cell-free biosensors: Principle, mechanism and applications. *Biotechnol. J.* **2020**, *15*, No. 2000187.

(5) Walde, P.; Cosentino, K.; Engel, H.; Stano, P. Giant vesicles: preparations and applications. *ChemBioChem.* **2010**, *11*, 848−865.

(6) Boyd, M. A.; Kamat, N. P. Designing artificial cells towards a new generation of biosensors. *Trends Biotechnol.* **2021**, *39*, 927−939.

(7) Roth, A.; Breaker, R. R. The structural and functional diversity of metabolite-binding riboswitches. *Annu. Rev. Biochem.* **2009**, *78*, 305−334.

(8) Tabuchi, T.; Yokobayashi, Y. Cell-free riboswitches. *RSC Chem. Biol.* **2021**, *2*, 1430−1440.

(9) Martini, L.; Mansy, S. S. Cell-like systems with riboswitch controlled gene expression. *Chem. Commun.* **2011**, *47*, 10734−10736.

(10) Lentini, R.; Santero, S. P.; Chizzolini, F.; Cecchi, D.; Fontana, J.; Marchioretto, M.; Del Bianco, C.; Terrell, J. L.; Spencer, A. C.; Martini, L.; Forlin, M.; Assfalg, M.; Serra, M. D.; Bentley, W. E.; Mansy, S. S. Integrating artificial with natural cells to translate chemical messages that direct *E. coli* behaviour. *Nat. Commun.* **2014**, *5*, 4012.

(11) Adamala, K. P.; Martin-Alarcon, D. A.; Guthrie-Honea, K. R.; Boyden, E. S. Engineering genetic circuit interactions within and between synthetic minimal cells. *Nat. Chem.* **2017**, *9*, 431−439.
(12) Dwidar, M.; Seike, Y.; Kobori, S.; Whitaker, C.; Matsuura, T.; Yokobayashi, Y. Programmable artificial cells using histamine-responsive synthetic riboswitch. *J. Am. Chem. Soc.* **2019**, *141*, 11103−11114.
(13) Boyd, M. A.; Thavarajah, W.; Lucks, J. B.; Kamat, N. P. Robust and tunable performance of a cell-free biosensor encapsulated in lipid vesicles. *Sci. Adv.* **2023**, *9*, No. eadd6605.
(14) Ishii, Y.; Fukunaga, K.; Cooney, A.; Yokobayashi, Y.; Matsuura, T. Switchable and orthogonal gene expression control inside artificial cells by synthetic riboswitches. *Chem. Commun.* **2024**, *60*, 5972−5975.
(15) Sawasaki, T.; Ogasawara, T.; Morishita, R.; Endo, Y. A cell-free protein synthesis system for high-throughput proteomics. *Proc. Natl. Acad. Sci. U.S.A.* **2002**, *99*, 14652−14657.
(16) Takahashi, H.; Ogawa, A. Coupled *in vitro* transcription/translation based on wheat germ extract for efficient expression from PCR-generated templates in short-time batch reactions. *Bioorg. Med. Chem. Lett.* **2021**, *52*, No. 128412.
(17) Ogawa, A. Biofunction-assisted sensors based on a new method for converting aptazyme activity into reporter protein expression with high efficiency in wheat germ extract. *ChemBioChem.* **2009**, *10*, 2465−2468.
(18) Ogawa, A. Rational design of artificial riboswitches based on ligand-dependent modulation of internal ribosome entry in wheat germ extract and their applications as label-free biosensors. *RNA* **2011**, *17*, 478−488.
(19) Ogawa, A. Rational construction of eukaryotic OFF-riboswitches that downregulate internal ribosome entry site-mediated translation in response to their ligands. *Bioorg. Med. Chem. Lett.* **2012**, *22*, 1639−1642.
(20) Ogawa, A. Ligand-dependent upregulation of ribosomal shunting. *ChemBioChem.* **2013**, *14*, 1539−1543.
(21) Ogawa, A.; Murashige, Y.; Tabuchi, J.; Omatsu, T. Ligand-responsive upregulation of 3′ CITE-mediated translation in a wheat germ cell-free expression system. *Mol. BioSyst.* **2017**, *13*, 314−319.
(22) Ogawa, A.; Masuoka, H.; Ota, T. Artificial OFF-riboswitches that downregulate internal ribosome entry without hybridization switches in a eukaryotic cell-free translation system. *ACS Synth. Biol.* **2017**, *6*, 1656−1662.
(23) Ogawa, A.; Murashige, Y.; Takahashi, H. Canonical translation-modulating OFF-riboswitches with a single aptamer binding to a small molecule that function in a higher eukaryotic cell-free expression system. *Bioorg. Med. Chem. Lett.* **2018**, *28*, 2353−2357.
(24) Ogawa, A.; Itoh, Y. *In vitro* selection of RNA aptamers binding to nanosized DNA for constructing artificial riboswitches. *ACS Synth. Biol.* **2020**, *9*, 2648−2655.
(25) Takahashi, H.; Okubo, R.; Ogawa, A. Eukaryotic artificial ON-riboswitches that respond efficiently to mid-sized short peptides. *Bioorg. Med. Chem. Lett.* **2022**, *71*, No. 128839.
(26) Ogawa, A.; Inoue, H.; Itoh, Y.; Takahashi, H. Facile expansion of the variety of orthogonal ligand/aptamer pairs for artificial riboswitches. *ACS Synth. Biol.* **2023**, *12*, 35−42.
(27) Takahashi, H.; Fujikawa, M.; Ogawa, A. Rational design of eukaryotic riboswitches that up-regulate IRES-mediated translation initiation with high switching efficiency through a kinetic trapping mechanism in vitro. *RNA* **2023**, *29*, 1950−1959.
(28) Ogawa, A.; Fujikawa, M.; Onishi, K.; Takahashi, H. Cell-free biosensors based on modular eukaryotic riboswitches that function in one pot at ambient temperature. *ACS Synth. Biol.* **2024**, *13*, 2238−2245.
(29) Sasaki, J.; Nakashima, N. Translation initiation at the CUU codon is mediated by the internal ribosome entry site of an insect picorna-like virus in vitro. *J. Virol.* **1999**, *73*, 1219−1226.
(30) Ogawa, A.; Takamatsu, M. Mutation of the start codon to enhance *Cripavirus* internal ribosome entry site-mediated translation in a wheat germ extract. *Bioorg. Med. Chem. Lett.* **2019**, *29*, No. 126729.
(31) Pfingsten, J. S.; Kieft, J. S. RNA structure-based ribosome recruitment: Lessons from the *Dicistroviridae* intergenic region IRESes. *RNA* **2008**, *14*, 1255−1263.
(32) Hirano, M.; Ando, R.; Shimozono, S.; Sugiyama, M.; Takeda, N.; Kurokawa, H.; Deguchi, R.; Endo, K.; Haga, K.; Takai-Todaka, R.; Inaura, S.; Matsumura, Y.; Hama, H.; Okada, Y.; Fujiwara, T.; Morimoto, T.; Katayama, K.; Miyawaki, A. A highly photostable and bright green fluorescent protein. *Nat. Biotechnol.* **2022**, *40*, 1132−1142.
(33) Jenison, R. D.; Gill, S. C.; Pardi, A.; Polisky, B. High-resolution molecular discrimination by RNA. *Science* **1994**, *263*, 1425−1429.
(34) Takahashi, H.; Ogawa, A. Preparation of a millimeter-sized supergiant liposome that allows for efficient, eukaryotic cell-free translation in the interior by spontaneous emulsion transfer. *ACS Synth. Biol.* **2020**, *9*, 1608−1614.
(35) Takahashi, H.; Ogawa, A. A detailed protocol for preparing millimeter-sized supergiant liposomes that permit efficient eukaryotic cell-free translation in the interior. *Bio-Protocol* **2021**, *11*, No. e4054.
(36) Uyeda, A.; Reyes, S. G.; Kanamori, T.; Matsuura, T. Identification of conditions for efficient cell-sized liposome preparation using commercially available reconstituted *in vitro* transcription-translation system. *J. Biosci. Bioeng.* **2022**, *133*, 181−186.
(37) Lis, L. J.; Lis, W. T.; Parsegian, V. A.; Rand, R. P. Adsorption of divalent cations to a variety of phosphatidylcholine bilayers. *Biochemistry* **1981**, *20*, 1771−1777.
(38) Gonzales, D. T.; Yandrapalli, N.; Robinson, T.; Zechner, C.; Tang, T-Y. D. Cell-free gene expression dynamics in synthetic cell populations. *ACS Synth. Biol.* **2022**, *11*, 205−215.
(39) Sigler, A.; Schubert, P.; Hillen, W.; Niederweis, M. Permeation of tetracyclines through membranes of liposomes and *Escherichia coli*. *Eur. J. Biochem.* **2000**, *267*, 527−534.
(40) Takahashi, S.; Inamura, K.; Yarimizu, J.; Yamazaki, M.; Murai, N.; Ni, K. Neurochemical and neuropharmacological characterization of ASP2905, a novel potent selective inhibitor of the potassium channel KCNH3. *Eur. J. Pharmacol.* **2017**, *810*, 26−35.
(41) Müller, M.; Weigand, J. E.; Weichenrieder, O.; Suess, B. Thermodynamic characterization of an engineered tetracycline-binding riboswitch. *Nucleic Acids Res.* **2006**, *34*, 2607−2617.
(42) Gadella, T. W. J., Jr.; van Weeren, L.; Stouthamer, J.; Hink, M. A.; Wolters, A. H. G.; Giepmans, B. N. G.; Aumonier, S.; Dupuy, J.; Royant, A. mScarlet3: a brilliant and fast-maturing red fluorescent protein. *Nat. Methods* **2023**, *20*, 541−545.
(43) Fukunaga, K.; Dhamodharan, V.; Miyahira, N.; Nomura, Y.; Mustafina, K.; Oosumi, Y.; Takayama, K.; Kanai, A.; Yokobayashi, Y. Small-molecule aptamer for regulating RNA functions in mammalian cells and animals. *J. Am. Chem. Soc.* **2023**, *145*, 7820−7828.
(44) Hall, M. P.; et al. Engineered luciferase reporter from a deep sea shrimp utilizing a novel imidazopyrazinone substrate. *ACS Chem. Biol.* **2012**, *7*, 1848−1857.
(45) Noireaux, V.; Libchaber, A. A vesicle bioreactor as a step toward an artificial cell assembly. *Proc. Natl. Acad. Sci. U.S.A.* **2004**, *101*, 17669−17674.
(46) Ogawa, A.; Tabuchi, J.; Doi, Y. Identification of short untranslated regions that sufficiently enhance translation in high-quality wheat germ extract. *Bioorg. Med. Chem. Lett.* **2014**, *24*, 3724−3727.
(47) Ogawa, A. Rational design of artificial ON-riboswitches. *Methods Mol. Biol.* **2014**, *1111*, 165−181.
(48) Toyota, T.; Zhang, Y. Effect of an oil medium on giant vesicles prepared with water-in-oil emulsion. *Bunseki Kagaku* **2022**, *71*, 83−89.

https://doi.org/10.1021/acssynbio.4c00696
ACS Synth. Biol. 2025, 14, 771−780